Numerical investigation of the response of expansion anchors used to attach helical pile connectors to concrete foundations

M.M. El Sharnouby and M.H. El Naggar

Abstract: This paper evaluates the performance of expansion anchors used to attach helical pile connectors to foundations. The anchors' response to pullout loads was evaluated using nonlinear finite element analysis with the aid of the commercial software, Abaqus. The connector capacity under horizontal movement of the foundation for different anchor diameters, embedment depths, and anchors' spacing is reported. It was found that the pre-tension load had no influence on the anchor ultimate capacity, but affected the anchor response at service load levels and the displacement at failure. Under pullout loading, increasing the anchor diameter resulted in a more brittle response, but did not affect the ultimate capacity when the concrete tensile strength dominated the response. No interaction between anchors was observed for spacing ≥ 1.67 times the anchor's embedment depth. A modification to the helical pile connector configuration is proposed.

Key words: helical pile, specialized connector, cracking, expansion anchor, finite element, Abaqus.

Résumé : Cet article évalue le rendement des coquilles d'expansion utilisées pour attacher les connecteurs des pieux hélicoïdaux aux fondations. La réaction des coquilles d'expansion aux charges d'arrachement a été évaluée par analyse des éléments finis non linéaires en utilisant le progiciel commercial Abaqus. La capacité du connecteur est signalée pour un mouvement horizontal de la fondation pour différents diamètres de coquille d'expansion, de profondeur d'enfouissement et d'espacement des coquilles d'expansion. Il a été remarqué que la charge de précontrainte n'a aucune influence sur la capacité de la coquille d'expansion à la rupture, mais qu'elle a affecté la réaction des coquilles d'expansion en ce qui concerne les charges de service et le déplacement à la rupture. L'augmentation du diamètre de la coquille d'expansion sous une charge d'arrachement a engendré une réponse plus cassante mais n'a pas affecté la capacité à la rupture lorsque la résistance en tension du béton domine la réaction. Aucune interaction entre les coquilles d'expansion n'a été observée pour un espacement ≥ 1,67 fois la profondeur d'enfouissement des coquilles d'expansion. Une modification à la configuration des connecteurs des pieux hélicoïdaux est proposée.

Mots-clés : pieu hélicoïdal, connecteur spécialisé, fissuration, coquille d'expansion, éléments finis, Abaqus.

[Traduit par la Rédaction]

1. Introduction

Helical screw piles are used as an efficient retrofit technique for low-rise residential and commercial buildings (Carville and Walton 1995). Helical piles are attached to the existing foundation using a two-piece specialized connector. Typically, two wedge-type expansion anchors are utilized to attach the connector (bracket) to the foundation. When the foundation is subjected to horizontal loading, the connector relies on the pullout capacity of the two-wedge type expansion anchors connecting it to the foundation.

Expansion anchors transfer tensile loads to the concrete foundation via friction. The load transfer mechanism induces tensile stresses in the concrete. Hence, expansion anchors may fail by concrete cone breakout or splitting failure of the concrete. Other failure modes include anchor steel fracture, pull-through, and pullout. All analytical methods that are developed based on experimental data are suitable for design purposes only when failure is controlled by concrete breakout or steel failure modes. To investigate all possible failure modes, experimental or numerical investigations need to be conducted. In this paper, nonlinear finite element analysis (FEA) is used to establish the load–displacement behaviour of wedge-type expansion anchors in uncracked concrete subjected to pullout load and to perform parametric studies. The analyses are carried out using the commercial software, Abaqus (Hibbitt et al. 2008).

The load–deflection behaviour and failure mode of an expansion anchor depends on several parameters including: the pre-tension load, anchor diameter, embedment depth, edge distance, and the concrete behaviour in tension. The parametric study presented here investigates the influence of different factors on the anchors response. Anchors with diameters of 12.7 and 15.9 mm were investigated. The embedment depth varied from 4.5 to 9 times the anchor diameter. The case of connectors with two anchors (double

Received 14 October 2008. Revision accepted 23 February 2010. Published on the NRC Research Press Web site at cjce.nrc.ca on 9 June 2010.

M.M. El Sharnouby and M.H. El Naggar.[1] Department of Civil and Environmental Engineering, The University of Western Ontario, London, ON N6A 5B9, Canada.

Written discussion of this article is welcomed and will be received by the Editor until 31 October 2010.

[1]Corresponding author (e-mail: helnaggar@eng.uwo.ca).

Fig. 1. dimensions of the 12.7 mm (1/2 in) and the 15.9 mm (5/8 in) anchors.

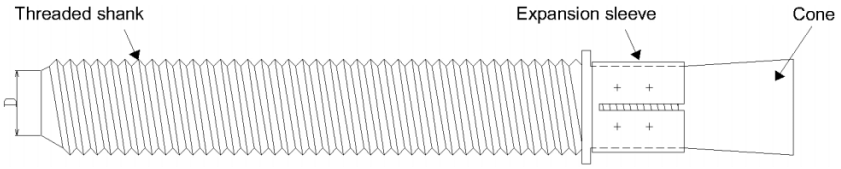

Fig. 2. Edge and spacing distances for typical anchor installation.

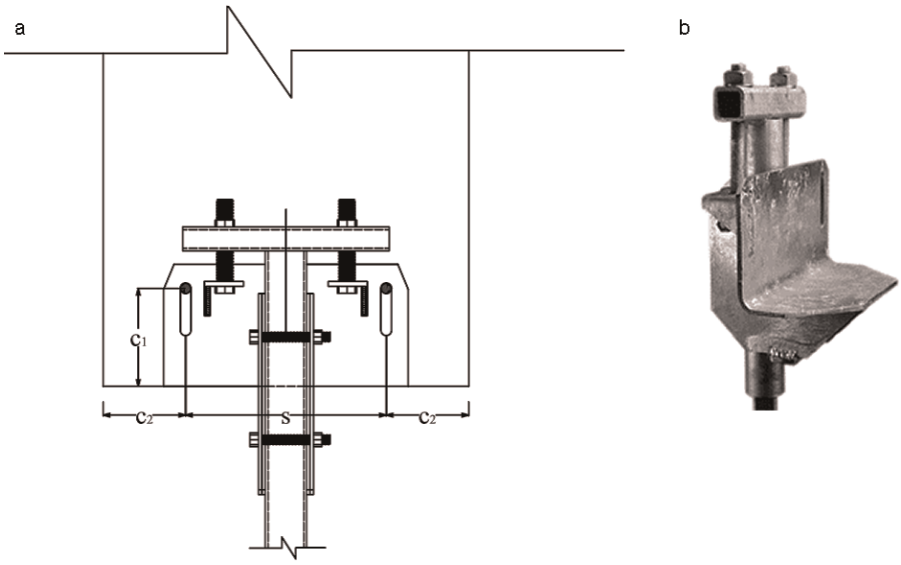

anchorage systems) was also analyzed to examine the possibility of upgrading the connector capacity.

2. Anchors and parameters studied

The anchors typically used to fasten the connector to the concrete foundation are hot-dipped galvanized torque-controlled expansion anchors (Fig. 1). They are composed of an anchor shaft, an expansion sleeve, and a conical end. The investigated anchors are made of steel with a yield strength, f_y, of 380 MPa and a tensile strength, f_{ut}, of 517 MPa (ESR-2251). The connector design allows the installation of anchors with diameters 12.7 mm (1/2 in) and 15.9 mm (5/8 in). In the following sections, anchors will be identified based on their size. For the 12.7 mm, d_1 = 12.7 mm, d_2 = 11.35 mm, and l_s = 12.5 mm. For the 15.9 mm anchor: d_1 = 15.8 mm, d_2 = 14.5 mm, and l_s = 15.9 mm.

2.1 Anchor installation configuration

The investigated expansion anchors are typically installed with an effective embedment depth, h_{eff} equal to six times its diameter, d; i.e., h_{eff} = 6d. In the current investigation, the embedment depth varied from h_{eff} = 4.5–9d, for single anchor cases. For double anchorage cases, it varied from h_{eff} = 6–9d. In current installation practice, the connector's anchors are installed with an edge distance, c_1, which varies between 60 and 120 mm (Figs. 2*a* and 2*b*). The edge distance in other directions depends on the foundation size and piles' spacing. The edge distance c_1 = 120 mm was considered for all models, and in other directions, c_2 was kept larger than 1.5h_{eff}.

In practice, the anchors are spaced at a distance s = 292.1 mm (11.5 in). In this study, for double anchorage cases, spacing was varied between s = 152.2 and 292.1 mm for the 12.7 mm anchor (h_{eff} = 6d) and from s = 240 to 292.1 mm for the 15.9 mm anchor (h_{eff} = 9d).

3. Parameters selection for finite element analysis

This section provides concrete and steel parameters used in this study. Parameter selection was based on results from previous experiments, parameters used in previous FEA and concrete plastic-damage models, and developed empirical equations.

3.1 Concrete parameters

Concrete parameters used in this study are: concrete compressive strength $f'_c = 25$ MPa (as typically used in house foundations), compression modulus of elasticity $E_c = 4800\sqrt{f'_c}$ MPa, Poisson's ratio, ν_c, = 0.2, yield limit $f_{cy} = 0.5f'_c$, strain at ultimate stress, ϵ_{cu}, = 0.0015, concrete tensile strength $f_t = 0.1f'_c$, biaxial to uniaxial compressive ratio f_{bu}/f_{cu} = 1.16 (Kupfer et al. 1969), and the ratio of the second stress invariant on the tensile meridian to that on the compressive meridian for a given value of the first stress invariant K_c = 2/3 (Lubliner et al. 1989). Compressive behaviour was described by a bilinear stress–strain relationship as shown in Fig. 3*a*, with the compressive damage parameter

Fig. 3. Concrete model: (*a*) compression; (*b*) tension no cracking; (*c*) stress-cracking displacement.

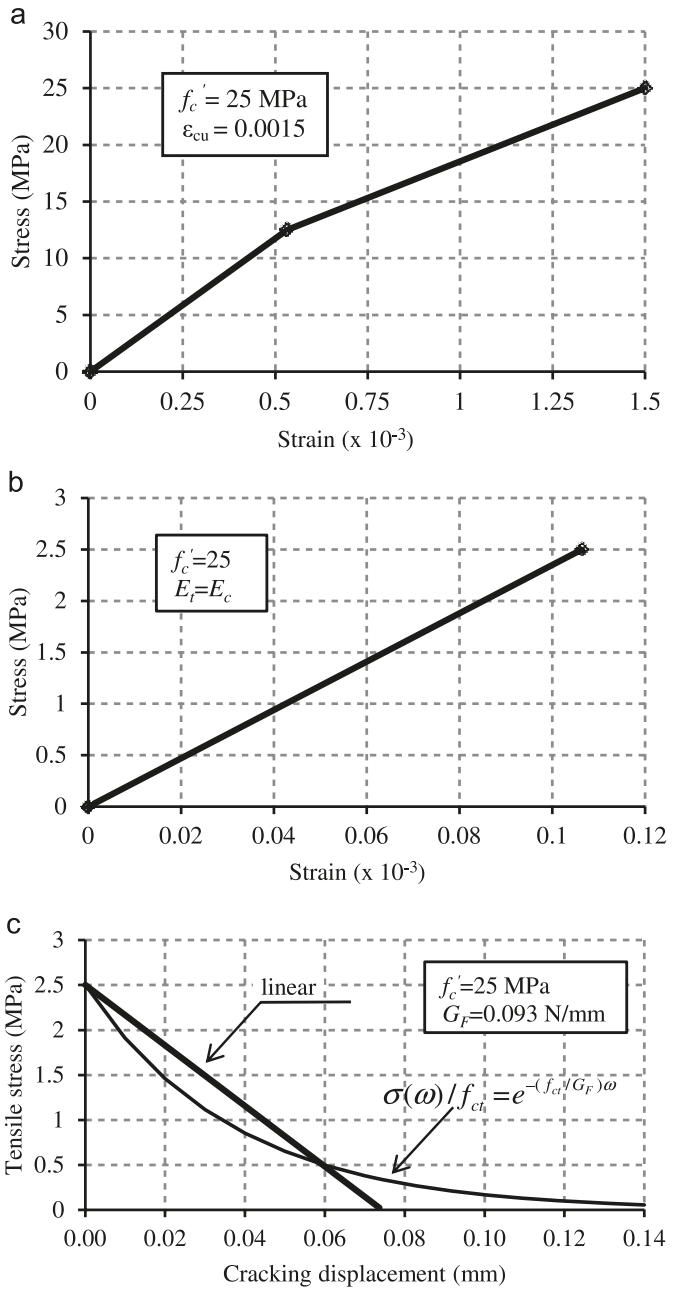

equal to zero. The tensile behaviour was described by a linear stress–strain curve until cracking, considering the tension modulus of elasticity $E_t = E_c$ (Fig. 3*b*) and damage parameter $d_t = 0.75$.

Post cracking behaviour was described by a stress-cracking displacement relationship (σ–ω). The equations proposed by Bazant and Becq-Giraudon (2002) for evaluating G_F were adopted, with: $\alpha_o = 1.44$, $d_a = 16$ mm, and $\omega/c = 0.5$ yielding $G_F = 0.093$ N/mm. Both linear and exponential stress-cracking displacement relationships were considered, where G_F was kept constant as shown in Fig. 3*c*. In the case of the exponential σ–ω shape, the formula proposed by Eligehausen et al. (2006) was adopted: $\sigma(\omega)f_{ct} = e^{-(f_{ct}/G_F)\cdot\omega}$,

Fig. 4. Stress–strain model for anchor and sleeve (steel).

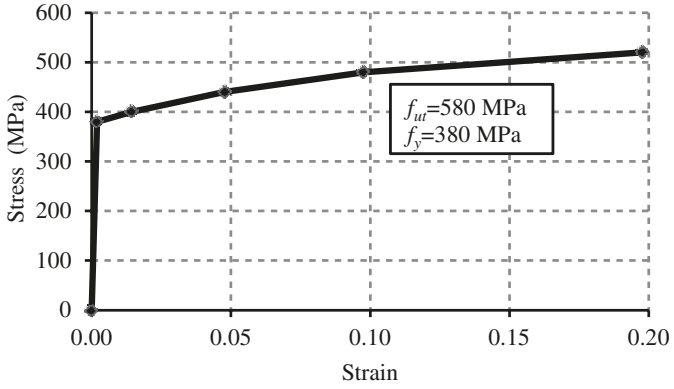

and ω_c, the displacement corresponding to $\sigma(\omega) = 0$ was taken as 0.14–0.2 mm (Reinhardt 1997, according to Eligehausen et al. 2006).

A parametric study was performed to determine the influence of the stress-cracking displacement relationship and it was found that implementing a linear σ-ω shape in FEA may lead to unconservative results in comparison with exponential σ–ω. Therefore, the exponential relationship is used in this study.

3.2 Steel parameters

A multilinear stress–strain relationship was used in this analysis to describe the behaviour of the anchor and the sleeve (Fig. 4). The steel parameters were taken as: Young's modulus E_s = 200 GPa, Poisson's ratio $\nu_s = 0.3$, yield stress f_y = 380 MPa, and ultimate strength f_{ut} = 517 MPa (ICC 2007). The coefficient of friction between steel and steel, μ_s, was assumed as 0.16 and between hardened concrete and steel, $\mu_c = 0.43$ (Cook and Klingner 1989).

4. Geometry and model discretization

The anchorage system was simulated using a 3D finite element (FE) model comprised of eight-nodded hexahedron elements, C38DR, to represent the concrete foundation, the anchor (shaft and nut), and the sleeve. Reduced integration elements were chosen, as opposed to fully integrated elements, to overcome the volumetric locking effect of the fully integrated elements when material model is almost incompressible (Cook et al. 2002). A staged mesh refinement was carried out to reach an optimum solution. To accurately capture the geometry of the anchor, the average aspect ratio of elements was kept below 1:4. In high stress concentration regions, the aspect ratio was kept close to unity. No yielding is expected in the connector itself; therefore, it was treated as rigid.

To reduce the computational time and effort, with acceptable accuracy, the anchorage system was simplified to rectangular half symmetric circular and rectangular models as shown in Figs. 5*a* and 6*a*. A fully fixed boundary condition was applied to the base of the foundation. In addition, symmetry boundary conditions were employed, i.e., only half of the system is modeled. A typical FE mesh is shown in Figs. 5*b* and 6*b* for single and double anchorage cases, respectively.

Fig. 5. (*a*) Single anchorage system geometry. (*b*) Single anchorage system typical finite element mesh.

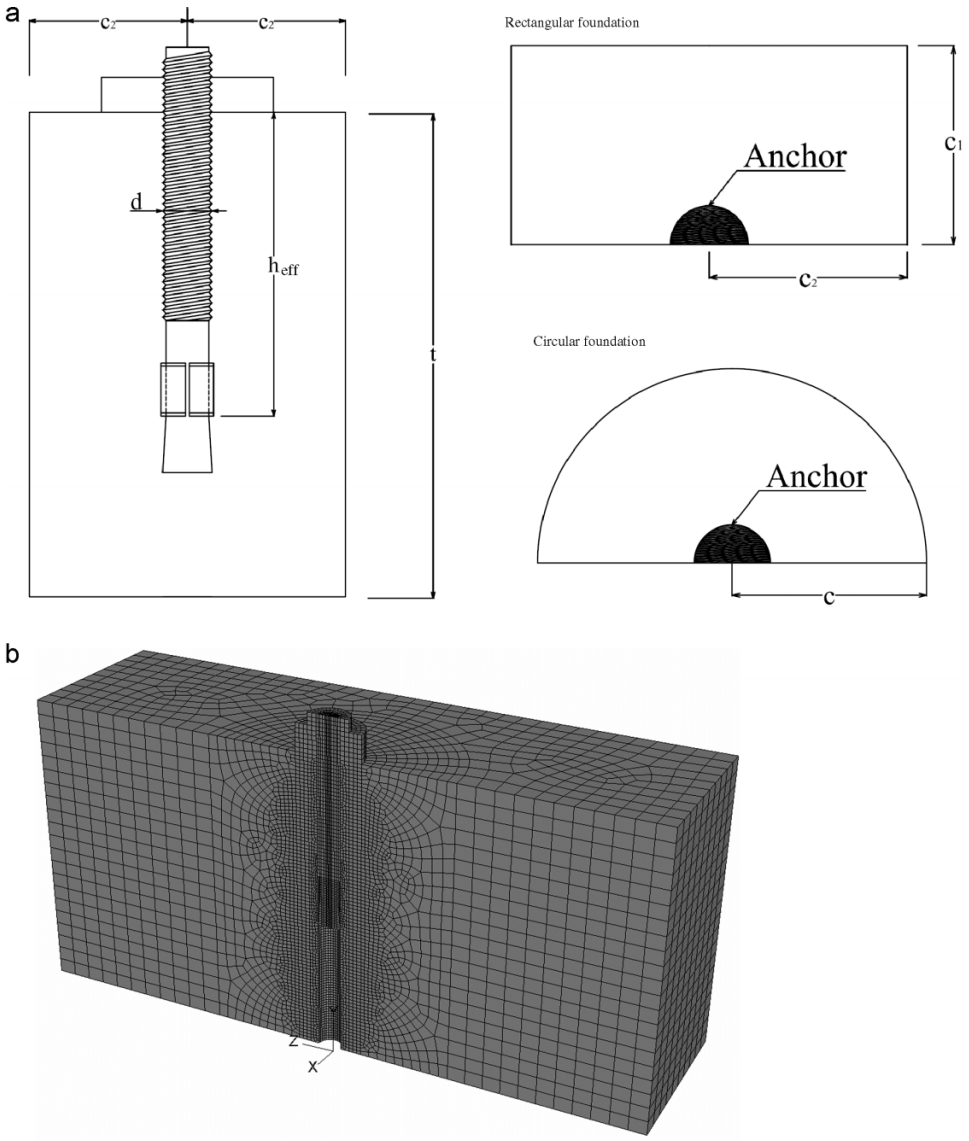

5. Verification of the finite element model

The verification of the FE model was accomplished by comparing the results of the FEA with the results from the experimental study performed by Cattaneo (2007). The experimental study involved single wedge-type expansion anchors subjected to tensile loading embedded in unreinforced concrete. The anchor had a diameter d = 12 mm, yield strength f_y = 544 MPa and tensile strength f_{ut} = 640 MPa.

Figure 7 compares the load–displacement curves obtained from the numerical model with the experimental load–displacement curve (Cattaneo 2007). Initially, both curves show very high stiffness. The experiment curve then shows a small displacement before the anchor starts to slip. This is probably due to the vertical deformation in the loading plate or the relative movement between the nut and the anchor threads. These factors have not been considered in the FEA. After reaching the pre-tension load, the "post-yield" response of the anchorage system predicted from the FEA coincides with that observed from the experiment. Note that the term "post-yield" is a term used to characterize anchor response subsequent to the initial linear load–displacement behaviour. This response is not associated with yielding of the anchor steel. However, as the loading continued, the FEA predicts a slightly stiffer response. This might be due to the fact that in the load transfer zone, the concrete is severely damaged due to high compressive forces resulting from the expansion mechanism. It should be noted that the damage and softening phenomena of concrete have not been taken into account in the current FE model.

The fact that the linear and exponential stress–displacement curves gave similar results shows that the failure was dominated by the pull-through mechanism and not dependent on the tensile strength of the concrete. In conclusion,

Fig. 6. (*a*) Double anchorage system geometry. (*b*) Double anchorage system typical finite element mesh.

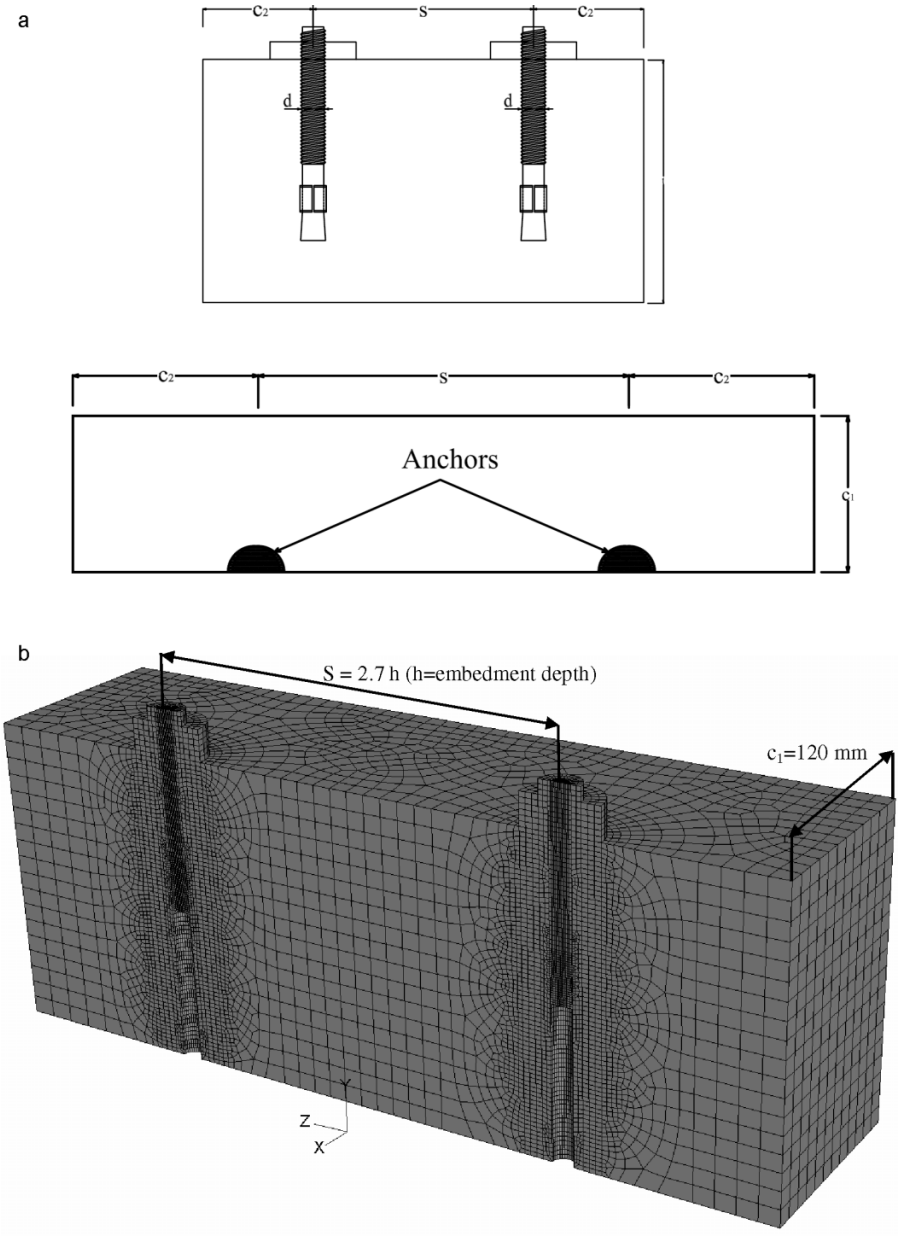

the load–displacement behaviour, the ultimate load, and the displacement at failure have been predicted very well by the FE model for the case of pull-through failure.

6. Failure mechanism and modes

Depending on the anchor diameter, embedment depth, anchor spacing, and the shape of concrete tensile softening response, three failure modes under tensile loading were observed: pull-through (P), concrete splitting (S), and a combination of pull-through/splitting (P–S). Figure 8 shows a typical deformed shape for the pull-through failure mode. Figure 9 shows the crack pattern, represented by plotting the damage variable, for anchors failing by the splitting failure mode due to insufficient edge distance for a single anchorage case. Figure 10 shows the crack pattern, represented by the damage variable, for anchors failing by the splitting failure mode due to insufficient spacing distance for the double anchors case.

Circumferential cracks initiated underneath the sleeve when applying the pre-tension load (Fig. 11*a*). These conical cracks (shown by plotting the maximum principal strains) extended horizontally and vertically (in the loading direction, at the contact surface between the sleeve and the concrete) as the load increased (Fig. 11*b*). Before the ultimate load was reached, cracking initiated at the anchor surface due to high expansion forces and lack of confinement at the top. As the ultimate load was exceeded, the cracks started propagating vertically parallel to the anchor axis until it bridged with the conical cracks at the sleeve contact area while radial splitting cracks at the concrete surface started propagating towards the free edge. The cracking area in-

Fig. 7. Comparison of numerical and experimental load–displacement curves.

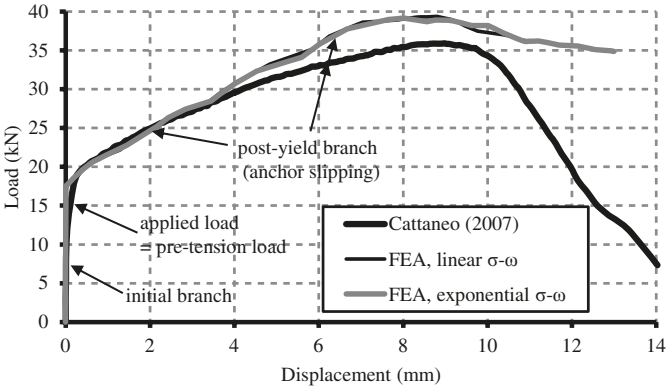

creased gradually until the load reached about 95% of the ultimate load (Fig. 11*c*) and accelerated afterwards. At ultimate load, discrete splitting cracks have not formed yet. As shown in Fig. 11*d*, further displacement caused the cracks to widen and to propagate rapidly until the splitting crack was completely formed (unstable crack growth).

Figures 12 and 13 show typical load–displacement curves at different locations for different failure modes. In these figures, the displacement of the anchor shank refers to the displacement measured at the plate top, whereas the anchor tip refers to that measured at the anchor conical end.

Under pullout loading, the anchors initially displayed very high stiffness (minimal displacement) until the applied load reaches the pre-tension value. Further increase in the load resulted in a repetitive process of the anchor slipping and setting into a new position (note the zigzag shape in the curves) until either of two failure modes occurred: the anchor is pulled completely through the sleeve, or the splitting force reached the splitting failure load of the concrete block. After failure, the anchor failing by pull-through continued to pull through the sleeve, producing a flat post-peak response. Anchors experiencing splitting failure displayed unstable crack propagation resulting in a steeper descending branch on load–displacement curve.

7. Influence of embedment depth

Figure 14 shows the load–displacement curves for different embedment depths for the 12.7 mm and 15.9 mm anchors considering both linear and exponential σ–ω relationships. In all cases, the anchors yielded when the applied load reached the pre-tension load. The slope of the post-yield stiffness increased with the increase of the embedment depth up to an embedment of 7.5*d*, and remained unchanged afterwards (i.e., the slope remained constant as the embedment was increased from 7.5*d* to 9*d*). It is also noted that increasing the embedment depth resulted in more ductile behaviour, except for the 12.7 mm anchor, and an embedment depth increase from 7.5*d* to 9*d*. It was observed that the failure mode was influenced by the embedment depth only in the cases where the exponential σ–ω relationship was utilized. For the 12.7 mm anchor, the failure mode was altered from splitting to pull-through/splitting for an increase in the embedment depth from 6*d* to 7.5*d*, and from

Fig. 8. Deformed shape and Misses stress (red zones are the highly stressed areas) distribution for pull-through failure mode.

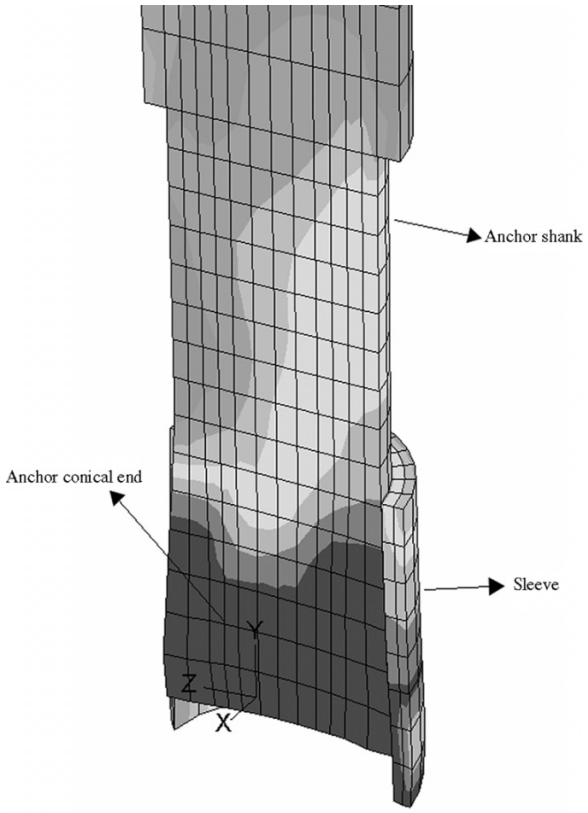

pull-through–splitting to pull-through for an increase in the embedment from 7.5*d* to 9*d*. For the 15.9 mm anchor, the anchor behaviour was dominated by the pull-through failure mode at an embedment of 9*d*.

Table 1 shows the percentage of the ultimate load and the ultimate displacement, with reference to that of the embedment depth of 7.5*d*. It can be noted from Table 1 that increasing the embedment depth from 4.5*d* to 7.5*d* resulted in an increase in the ultimate capacity by 30%–40% and an increase in the displacement at failure by 20%–60%. However, increasing the embedment depth beyond 7.5*d* did not result in any further increase in the anchor capacity nor in the displacement at failure, except for the 15.9 mm anchor where the ultimate load and the displacement at failure were increased by about 10% and 20%, respectively, for the exponential σ–ω relation.

8. Influence of anchor diameter

Figure 15 shows the load–displacement curves for both anchor diameters, considering the exponential σ–ω shape, for embedment depth equal to 57.2, 73, 95, and 115 mm. The load–displacement curves for the anchorage system utilizing the 15.9 mm anchor are characterized by a higher post-yield stiffness, which can be explained by the increase in the force required to expand the sleeve. However, the 15.9 mm anchor displayed a favourable effect, in terms of the ultimate capacity, only when the failure was dominated by the pull-through failure mode (for h_{eff} equal to 115 mm).

Fig. 9. Crack pattern (red zones) for splitting failure mode due to edge effect.

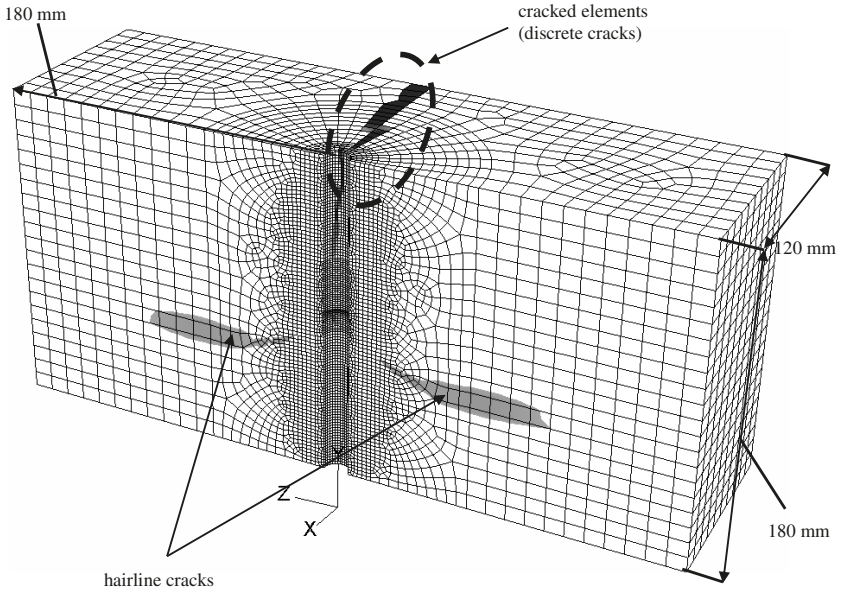

Fig. 10. Crack pattern (red zones) for splitting failure mode due to spacing effects.

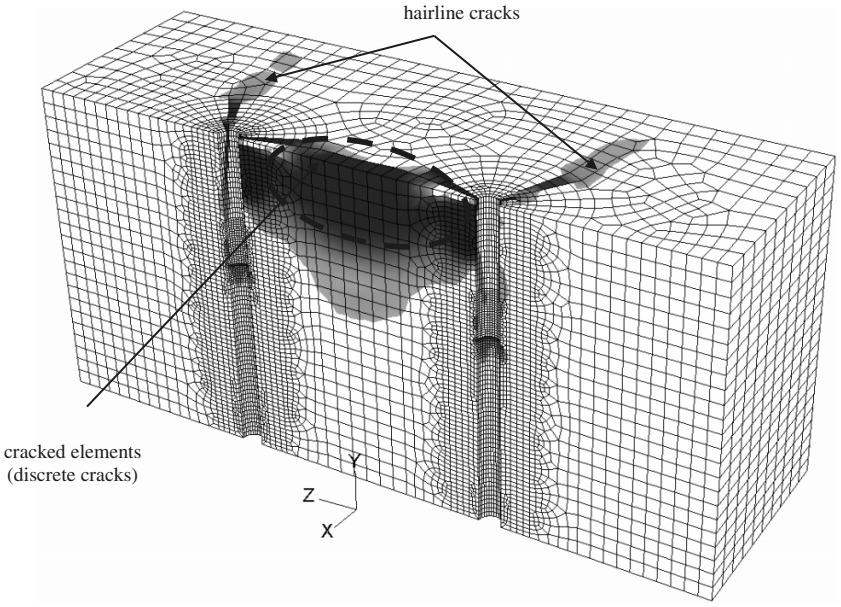

In cases where the 12.7 mm anchor failed by splitting, the 15.9 mm anchor produced the same failure mode, but with more brittle response.

Table 2 shows the percentage increase in the ultimate load and the displacement at ultimate load with respect to the 12.7 mm anchor. It can be seen that the 15.9 mm anchor increased the ultimate capacity by 13%–36% in cases where both anchors failed by pull-through. Otherwise (when other failure modes occurred or altered to a splitting failure mode), the ultimate load did not increase. In fact, for 73 mm embedment depth, the ultimate capacity was reduced by 14%. The same pattern can be observed for the displacement at failure, however the reduction due to the increase in the anchor diameter was greater compared with the reduction in the ultimate load. At 73 mm embedment depth, the 15.9 mm anchor showed a reduction of 51% in the ultimate displacement.

9. Influence of pre-tension load

Figure 16 shows the load–displacement curves for anchors having the same characteristics (d = 12.7 mm, h_{eff} = 6d), but different pre-tension loads (torques). It can be seen that the post-yield branches are basically parallel to each other. Both anchors failed under the same ultimate load, as expected, and consequently the anchor with the less pre-tension value

Fig. 11. Crack configuration at different loading stages: (*a*) after applying the pre-tension load, *P*, (*b*) at 95% of the ultimate load, (*c*) at 100% of the ultimate load, and (*d*) after failure.

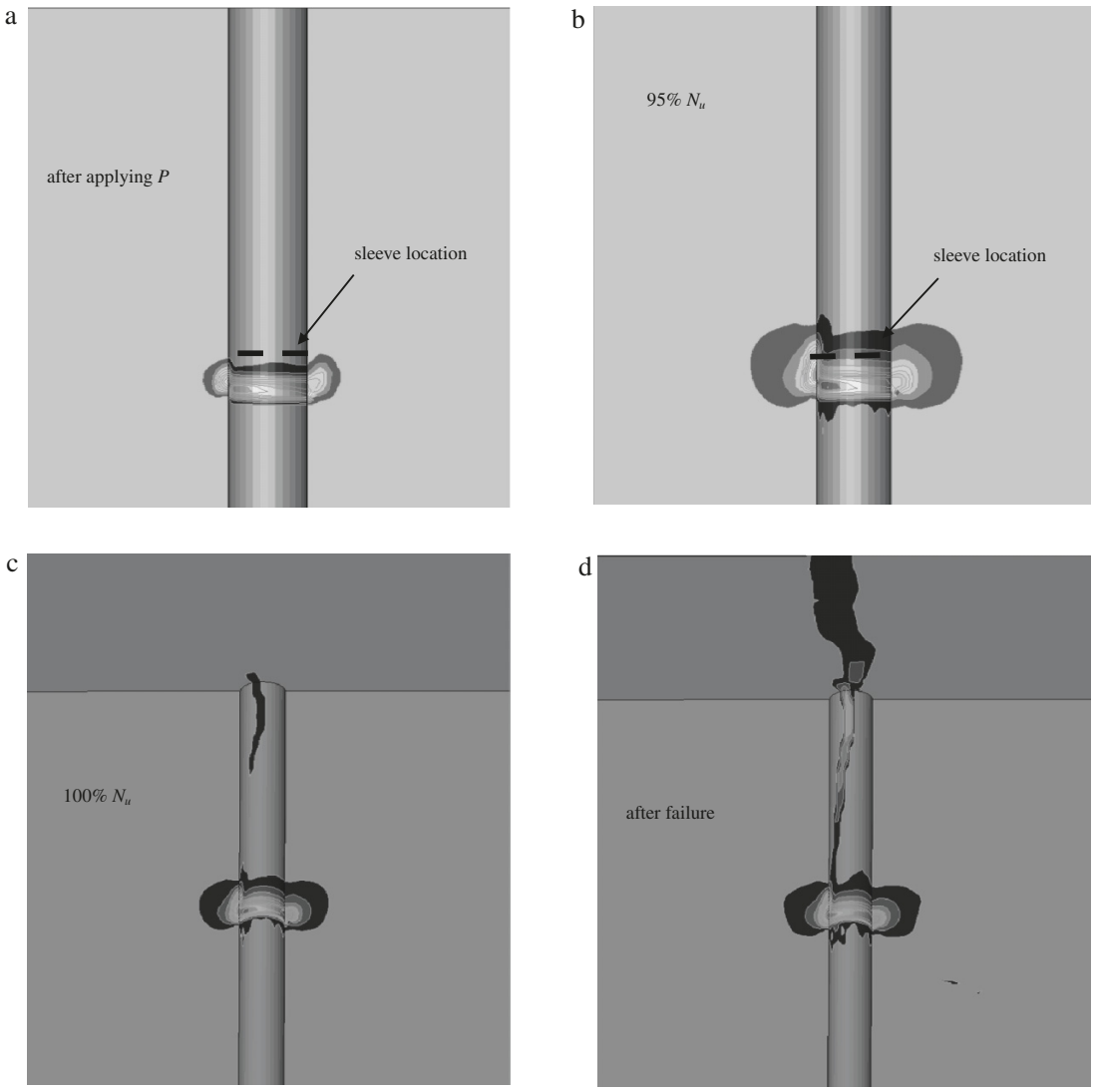

Fig. 12. Typical load–displacement curves at different locations for pull-through failure mode.

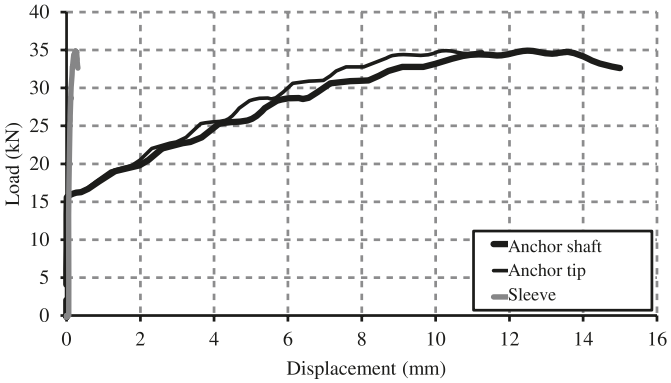

Fig. 13. Typical load–displacement curve at different locations for splitting failure mode.

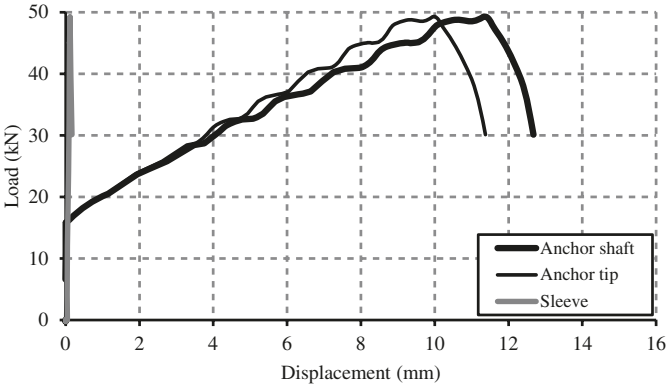

failed at a larger displacement. Therefore, anchors with higher pre-tension loads will have the same ultimate capacity, but less axial displacement at failure.

10. Influence of anchor spacing

Despite the observation that using an exponential σ–ω shape gives more conservative results, some analyses were

Fig. 14. Load–displacement curves for different embedment depths.

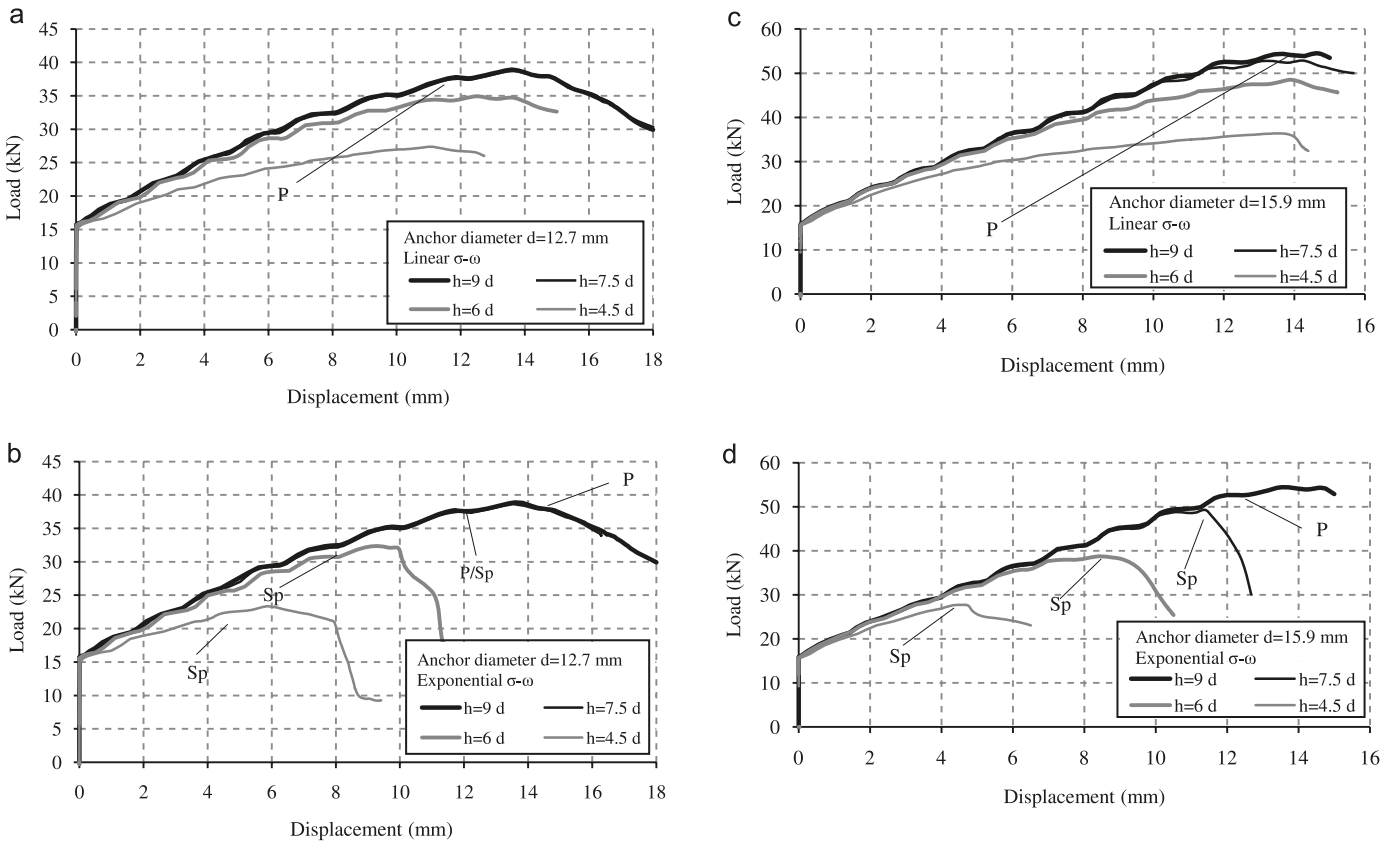

Table 1. Percentage of ultimate load with respect to ultimate load for anchors with $h = 7.5d$ for the 12.7 mm and the 15.9 mm anchors.

		Ultimate load (%)		Displacement at failure (%)	
Anchor diameter	Embedment depth	Linear σ–ω shape	Exponential σ–ω shape	Linear σ–ω shape	Exponential σ–ω shape
12.7 mm	4.5d	70.7	60.4	80.4	43.3
	6d	90.2	83.7	91.3	68.6
	7.5d	100	100	100	100
	9d	100.5	100.6	99.2	100.4
15.9 mm	4.5d	68.8	56.2	95.1	39.7
	6d	91.8	78.7	97.9	74.1
	7.5d	100	100	100	100
	9d	103	110.4	102.5	119.7

conducted on the 12.7 mm anchor ($h_{eff} = 6d$) with a spacing varying from $s = 2$–$4h_{eff}$ considering a linear σ–ω shape. This analysis was conducted to further explore the ability of the linear σ–ω shape to predict failure modes associated with relatively small edge distance and anchors' spacing. Figure 17 shows the load–displacement curves for different anchors' spacing. The splitting failure mode took place at a spacing of $2h_{eff}$ and $2.7h_{eff}$. At a spacing of $3.3h_{eff}$, the failure mode and ultimate load were identical to that of $s = 4h_{eff}$.

Similar analysis was conducted on the 15.9 mm anchor with spacings of 240 and 292.1 mm; the latter is currently used in practice. In both cases, the anchors failed by pull-through. Also, the anchors had almost the same ultimate load and displacement at failure as shown Table 3.

The critical spacing (minimum spacing to preclude splitting failure mode during loading) recommended by Eligehausen et al. (2006), based on Asmus' (Asmus 1999) results, is $s_{cr} = 2c_{cr}$, where $c_{cr} = 2.5h_{eff}$ ($s_{cr} = 5h_{eff}$) for torque-controlled expansion anchors with one expansion cone. The above results for the 15.9 mm anchor show that at spacing of $1.67h_{eff}$, no interaction between the anchors was observed, suggesting that using the above limits may lead to overly conservative design for deep embedment depths ($h_{eff} = 9d$). This limit is shown as $3.3h_{eff}$ for the 12.7 mm anchor of 6d embedment length.

Fig. 15. Load–displacement curves for different anchor diameters.

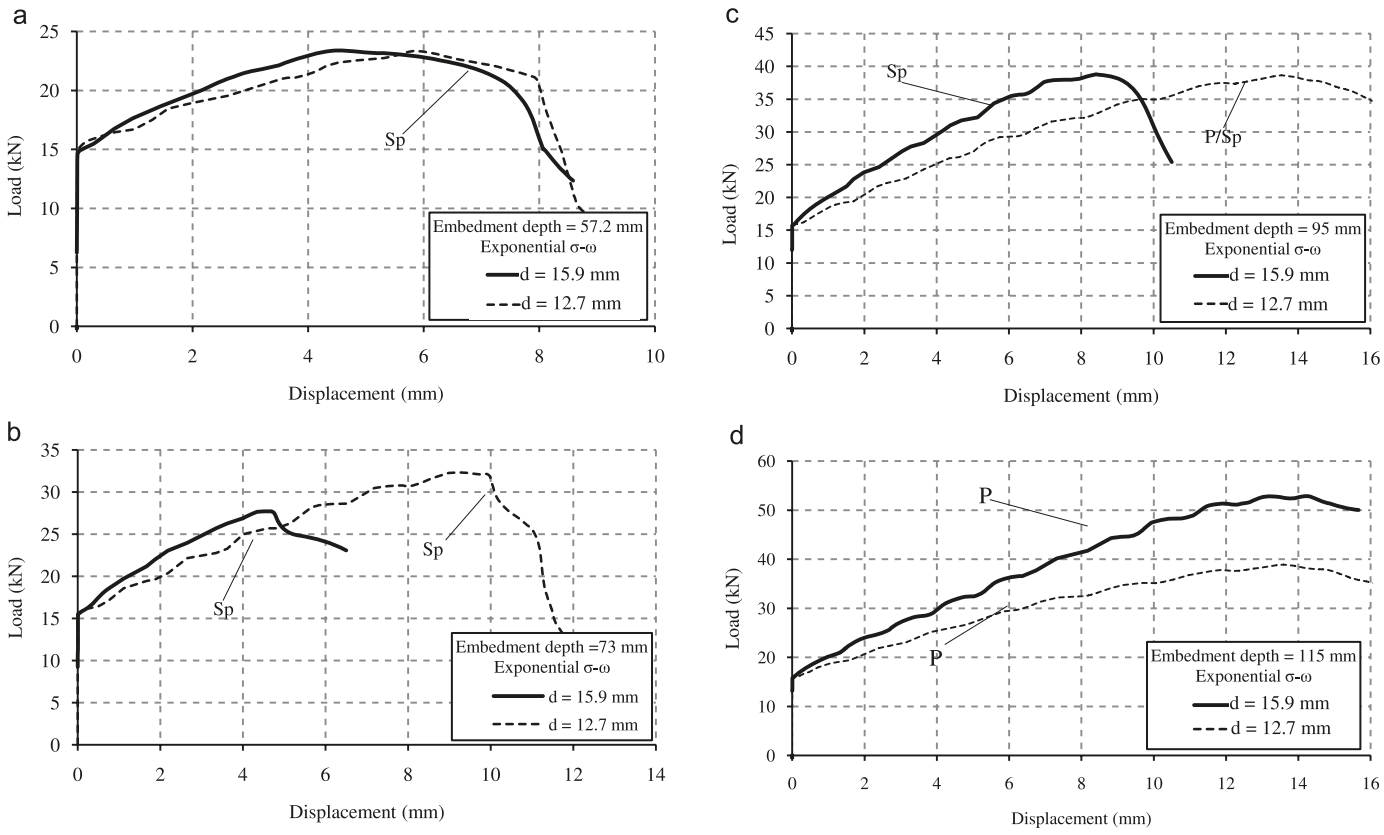

Table 2. Percentage of ultimate load and displacement at ultimate load with respect to the 12.7 mm anchor.

			Ultimate load (%)		Displacement at failure (%)	
σ–ω shape	Embedment depth (mm)	Embedment depth	12.7 mm*	15.9 mm*	12.7 mm	15.9 mm
Exponential	57.2	4.5*d*	100 (S)	100 (S)	100	78
	73	6*d*	100 (S)	86 (S)	100	49
	95	7.5*d*	100 (P/S)	100 (S)	100	62
	115	9*d*	100 (P)	127 (P)	100	83
Linear	57.2	4.5*d*	100 (P)	113 (P)	100	123
	73	6*d*	100 (P)	104 (P)	100	108
	95	7.5*d*	100 (P)	125 (P)	100	102
	115	9*d*	100 (P)	136 (P)	100	105

Note: S, splitting; P, pull-through.
*indicates failure mode.

11. Tensile capacity of the connector

The connector tensile capacity depends primarily on the two post-installed wedge-type expansion anchors. The discussion of the results of the two anchors' case shows that for the current anchor design (s = 292.1 mm) there is no group effect between the anchors. Therefore, the capacity of the connector is the sum of the tensile capacity of two individual anchors. Table 4 provides the ultimate capacity for the current connector configuration for all cases considered in the current study. It can be seen that the ultimate capacity for the 15.9 mm anchor with an embedment depth of 9*d* (108.9 kN) is slightly higher than the ultimate capacity of the RG-HSP helical pile (105 kN), reported by Abd-Elghany (2008).

12. Implementation in finite element model

The load–displacement curves established from the study of the anchor behaviour under pullout loading can be implemented in FEA to represent the tensile behaviour of the connector. All the load–displacement curves show that the connector response can be characterized by two distinct branches. In the first branch, the load increases with mini-

Fig. 16. Load–displacement curves for different pre-tension loads.

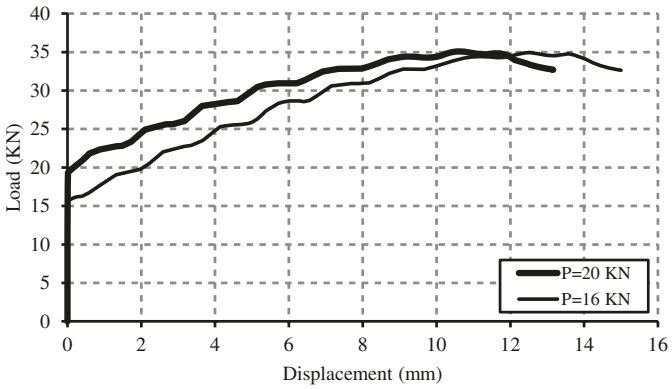

Fig. 17. Load–displacement curves for different anchor spacing.

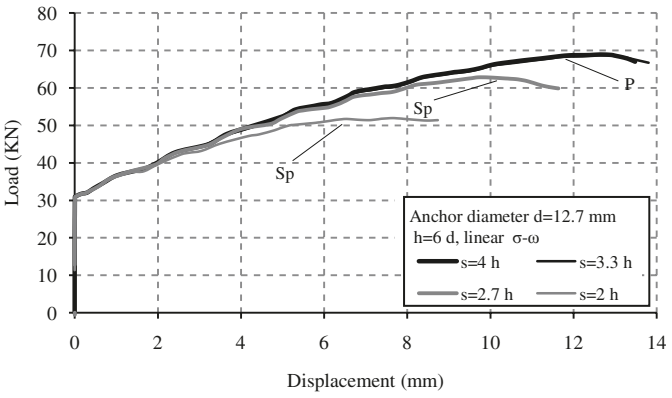

Table 3. Percentage of ultimate load and displacement at ultimate load for different anchors spacing.

Anchor diameter (mm)	Spacing (mm)	Ultimate load (%)	Displacement at failure (%)
15.9	292.1	100	100
	240	99.32	97.88

mal increase in the displacement, implying that the connector behaves as a rigid part up to the anchors' pre-tension load. When the applied load exceeds the pre-tension load, the connector starts displacing until the ultimate capacity is reached. Therefore, the tensile response of the connector, installed using the 12.7 mm or the 15.9 mm anchor for an embedment ranging from 4.5*d* to 9*d* and an edge distance of 120 mm can be modelled as a spring with a bilinear load–displacement relationship, as shown in Fig. 18. The slope of the first branch can be assigned a very high stiffness, e.g., ten times the stiffness of the structural element connected to the foundation. The second branch of the load–displacement curve can be defined by the pre-tension load, the ultimate load, and the displacement at failure predicted by the FEA.

13. Conclusions

In this paper, a parametric study on typical wedge-type expansion anchors, used to attach helical pile connectors to existing foundations, subjected to pull-out loading from a concrete foundation was conducted using the FE method. Based on the numerical analysis and the parametric study, the following conclusions can be made:

- Increasing the embedment depth resulted in an increase in the ultimate capacity and a more ductile behaviour of the anchorage, primarily as result of a shift in the failure mode from splitting to pull-through. For the 12.7 mm and the 15.9 mm anchors, the ultimate capacity of anchors installed at an embedment depth of nine times the diameter was higher by about 20% and 50% than those installed at an embedment depth of six times the anchor diameter (current installation practice), respectively. Similarly, the displacement at failure was increased by 45% and 60%. At an embedment depth of nine times the anchor diameter, the failure was dominated by the pull-through failure mode for both anchors.
- When the concrete tensile characteristics dominated the anchor response, increasing the anchor diameter resulted in a more brittle response and had no effect on the ultimate capacity. When the anchor response was governed by the expansion mechanism, anchors with larger diameter had higher ultimate capacity and displayed ductile behaviour.
- The pre-tension load has no influence on the anchor ultimate capacity, but affects only the anchor response at service load levels and the displacement at failure.
- For double anchorage cases, no interaction between the anchors was observed for spacing as low as 1.67 of the embedment depth, for the 15.9 mm anchor, installed at an embedment depth of 9*d* and an edge distance of 120 mm.

Table 4. Connector tensile capacity.

Anchor diameter, *d*	Embedment depth, *h*	FEA [kN] (failure mode)
12.7 mm (1/2 in)	4.5*d*	46.68 (S)
12.7 mm (1/2 in)	6*d*	64.65 (S)
12.7 mm (1/2 in)	7.5*d*	77.25 (P/S)
12.7 mm (1/2 in)	9*d*	77.76 (P)
15.9 mm (5/8 in)	4.5*d*	92.74 (S)
15.9 mm (5/8 in)	6*d*	72.72 (S)
15.9 mm (5/8 in)	7.5*d*	98.6 (S)
15.9 mm (5/8 in)	9*d*	108.9 (P)

Note: S, splitting; P/S, pull-through/splitting.

Fig. 18. Analytical model for the horizontal behaviour of the connector.

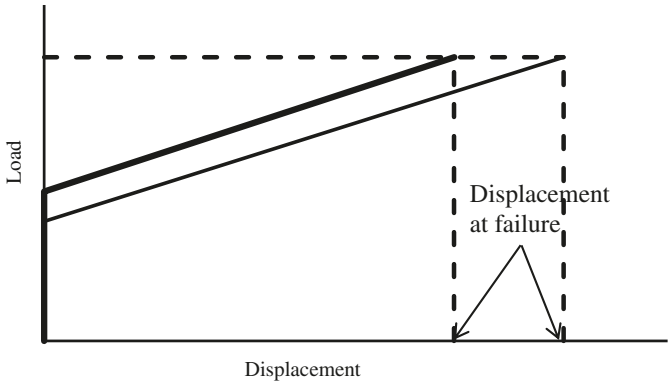

- The estimated capacities indicate that the helical pile connectors can sustain tensile loads up to 100 kN. The choice of anchor diameter and its embedment depth depends on the horizontal capacity of the helical pile.
- The overall behaviour of the foundation and the connector under horizontal loads can be modelled by a spring element having a bilinear load–displacement relationship.

It should be noted that the conclusions drawn in this study are applicable only for the strength and geometric parameters considered in the analysis. For the range of parameters considered, it is not recommended to install the anchors with an edge distance less than 120 mm.

Acknowledgments

The authors would like thank Dr. Sara Cattaneo for providing the experimental data for verification of the finite element model.

References

Abd-Elghany, Y. 2008. Monotonic and cyclic axial and lateral behaviour of helical piles. Ph.D. thesis, Faculty of Engineering, University of Western Ontario, London, Ont.

Asmus, J. 1999. Verhalten von Befestigungen bei der versagensart spalten des betons (Behavior of fasteners at concrete splitting). Ph.D. thesis, University of Stuttgart, Stuttgart, Germany. [In German.]

Bazant, Z.P., and Becq-Giraudon, E. 2002. Statistical prediction of fracture parameters of concrete and implications for choice of testing standard. Cement and Concrete Research, **32**(4): 529–556. doi:10.1016/S0008-8846(01)00723-2.

Carville, C.A., and Walton, R.W. 1995. Foundation repair using helical screw anchors. Proceedings of the Symposium on Foundation Upgrading and Repair for Infrastructure Improvement, San Diego, California, 23–26 October 1995. *Edited by* W.F. Kane and J.M. Tehaney. American Society of Civil Engineers (ASCE), New York. pp. 56–75.

Cattaneo, S. 2007. Wedge-type expansion anchors in high-performance concrete. ACI Structural Journal, **104**(2): 191–198.

Cook, R.A., and Klingner, R.E. 1989. Behavior and design of ductile multiple-anchor-to-concrete connections. Report 1126–3. Centre for Transportation Research, University of Texas at Austin, Austin, Tex.

Cook, R.D., Malkus, D.S., Plesha, M.E., and Witt, R.J. 2002. Concepts and applications of finite element analysis. 4th ed. John Wiley & Sons. Inc., New York.

Eligehausen, R., Mallee, R., and Silva, J.F. 2006. Anchorage in concrete construction. Ernst & Sohn, Berlin, Germany.

Hibbitt, H.D., Karlsson, B.I., and Sorensen, E.P. 2008. General purpose finite element analysis program, version 6.8. Habbitt, Karlsson & Sorensen, Inc., Pawtucket, R.I.

ICC. 2007. ITW red head trubolt carbon steel wedge anchors in concrete. Report ESR-2251. ICC Evaluation Service, Inc., Whittier, Calif.

Kupfer, H., Hilsdorf, H.K., and R sch, H. 1969. Behavior of concrete under biaxial stress. American Concrete Institute Journal, **66**(8): 656–666.

Lubliner, J., Oliver, J., Oller, S., and Oþate, E. 1989. A plastic-damage model for concrete. International Journal of Solids and Structures, **25**(3): 299–326.

Reinhardt, H.-W. 1997. Werkstoffe des bauwesens (Building materials). *In* Der Ingenieurbau. *Edited by* G. Mehlhorn. Ernst & Sohn, Berlin, Germany. [in German].